

## Article

# Hybrid TiO<sub>2</sub>-Polyaniline Photocatalysts and Their Application in Building Gypsum Plasters

Agnieszka Sulowska <sup>1\*</sup>, Izabela Wysocka <sup>1</sup>, Daniel Pelczarski <sup>2</sup> and Anna Zielińska-Jurek <sup>1\*</sup>

<sup>1</sup> Department of Process Engineering and Chemical Technology, Faculty of Chemistry, Gdansk University of Technology, 80-232 Gdansk, Poland

<sup>2</sup> Department of Physics of Electronic Phenomena, Faculty of Applied Physics and Mathematics, Gdansk University of Technology, 80-232 Gdansk, Poland

\* Correspondence: sulowska.as@gmail.com

**Abstract:** Hybrid materials of conjugated polymer and titanium(IV) oxide have attracted considerable attention concerning potential benefits, including (i) efficient exploitation of visible light, (ii) high adsorption capacity for organic contaminants, (iii) effective charge carriers separation. The new class of the photocatalysts is promising for the removal of environmental pollutants in both aqueous and gaseous phases. For the first time, in this study, the PANI/TiO<sub>2</sub> hybrid composite was used for the degradation of phenol in water and toluene in the gas phase. Polyaniline-TiO<sub>2</sub> was prepared by in-situ polymerization of aniline on the TiO<sub>2</sub> surface. The obtained hybrid material was characterized by diffuse reflectance spectroscopy (DR/UV-Vis), X-ray diffraction (XRD), fast-Fourier transformation spectroscopy (FTIR), photoluminescence (PL) spectroscopy, microscopy analysis (SEM/TEM) and thermogravimetric analysis (TGA). An insight into the mechanism was shown based on the photodegradation analysis of charge carriers scavengers. Polyaniline is an efficient TiO<sub>2</sub> photosensitizer for photodegradation in visible light ( $\lambda > 420$  nm). The trapping experiments revealed that mainly h<sup>+</sup> and <sup>•</sup>OH were reactive oxygen species responsible for phenol degradation. Furthermore, the PANI-TiO<sub>2</sub> hybrid nanocomposite was used in gypsum plaster to study the self-cleaning properties of the obtained building material. The effect of PANI-TiO<sub>2</sub> content on hydrophilic/hydrophobic properties and crystallographic structure of gypsum was studied. The obtained PANI-TiO<sub>2</sub> modified gypsum plaster had improved photocatalytic activity in the reaction of toluene degradation under Vis light.

**Keywords:** hybrid nanocomposites, polyaniline, titanium(IV) oxide, phenol, photocatalytic gypsum plaster

## 1. Introduction

Environmental pollution is one of the 21st-century major threats that negatively affect both human health and the entire ecosystem. Among currently available techniques for air and water purification, advanced oxidation processes (AOP) are efficient and environment-friendly technologies with a high oxidation potential to complete degradation of both organic and inorganic contaminants [1]. Among AOPs, heterogeneous photocatalysis is still of growing interest. The basis of photocatalysis consists of the excitation of semiconductors with energy greater or equal to its bandgap. As a result, the electron is transferred from the valence band to the conduction band, leaving the unoccupied positively charged energy state named hole. Photogenerated charge carriers participate in redox reactions with adsorbed water molecules, oxygen, and hydroxyl ions leading to the formation of reactive oxygen species capable of non-selective and effective oxidation of impurities [2].

The most commonly used photocatalytic semiconductors, including titanium(IV) oxide (TiO<sub>2</sub>) and zinc(II) oxide (ZnO), are activated under ultraviolet radiation, which requires application of

energy-consuming UV lamps, generating higher costs of purification, and limiting the use of green light sources such as sunlight. In this regard, the development of new photocatalysts active under visible light is highly demanded. The most common methods for modification of semiconductors include (i) surface modification with noble metal nanoparticles [3–6], (ii) doping with non-metals [7–9], and (iii) photosensitization with dyes [10,11]. Recently, conjugated polymers (CP) have become a new class of semiconductor materials with possible applications in photocatalytic degradation under visible light [12,13].

Hybrid nanomaterials based on the conjugated polymers such as polyaniline (PANI), polythiophene, polypyrrole or poly(3-hexylthiophene) and inorganic semiconductors can be applied for degradation of organic pollutants in aqueous phase [12–16]. Among conjugated polymers, polyaniline (PANI) is one of the most commonly used polymers due to good stability, non-toxicity, low synthesis cost, optical, and electrical properties and high electron mobility [17]. PANI hybrid nanocomposites are photocatalytic active under visible light due to HOMO-LUMO excitation and increased separation of electron-hole pairs [12]. A significant part of the research on photocatalytic activity of PANI-TiO<sub>2</sub> nanocomposites reported in the literature focused on the photodegradation reaction of dyes e.g. methylene blue [18] and Rhodamine B [19] in the aqueous phase. Moreover, there are only a few studies on the photocatalytic activity of PANI-TiO<sub>2</sub> nanocomposites in the gas phase reaction [20]. Degradation of pollutants in the gas phase is an important aspect. This approach allows for improving indoor air due to the more effective degradation of xenobiotics in air.

Furthermore, the obtained in this study hybrid photocatalyst was employed for the preparation of building material with self-cleaning properties. Most of the early studies focused on the addition of titanium(IV) oxide coupled with inorganic additives to obtain self-cleaning building materials [21–23]. Janus et al. [23] added nitrogen and carbon co-modified TiO<sub>2</sub> photocatalyst to commercial gypsum. The properties of the plaster were determined in RR198 dye degradation, as a model contaminant, under UV and UV-Vis light irradiation. The higher amount of anatase type photocatalysts present in the gypsum matrix increased the self-cleaning ability of modified gypsum material [23]. A recent study by Gnayem et al. [24] and Singh et al. [25] concluded that bismuth oxychloride (BiOCl) photocatalyst, which is active in visible light, could be used for the preparation of self-cleaning building material. Singh et al. [25] obtained cementitious containing 1% to 20% wt. BiOCl nanoparticles. The photocatalytic activity was analyzed in the reaction of the Resazurin decomposition under visible light irradiation. The results showed that photocatalytic performance improved linearly up to 5% of BiOCl addition in the cement matrix [25]. In particular, no study, to our knowledge, has considered using conjugated polymer-inorganic semiconductor hybrid nanocomposite in the building materials.

In this regard, PANI-TiO<sub>2</sub> composite was used for the first time, as an additive in plaster with photocatalytic properties. Also, the hydrophilic/hydrophobic properties of gypsums surfaces were measure during contact angle tests. The prepared gypsum samples were irradiated with a wavelength from the UV and visible region to evaluate photocatalytic activity in the gaseous phase during toluene degradation.

## 2. Materials and Methods

### 2.1. Materials

Aniline 98% (Sigma Aldrich, Saint. Louis, MO, USA), ammonium persulfate (Sigma Aldrich, Saint. Louis, MO, USA), hydrochloric acid 36,5% (POCh, Gliwice, Poland) were used, as starting materials, for the polymerization. As TiO<sub>2</sub> matrix titanium(IV) oxide P25 was supplied by Evonik (Evonik, Essen, Germany). Phenol was purchased from Sigma Aldrich (Sigma Aldrich, Saint. Louis, MO, USA) and selected as a model pollutant. Benzoquinone, ammonium oxalate, silver nitrate, and *tert*-butyl alcohol were also provided by Sigma Aldrich (Sigma Aldrich, Saint. Louis, MO, USA) and used as scavengers of superoxides, holes, electrons, and hydroxyl radicals, respectively. Acetonitrile (Merck, Darmstadt, Germany) and orthophosphoric acid (85%) (VWR, Gdansk, Poland) were used,

as eluents, for HPLC mobile phase. Ethylene glycol was purchased from Sigma Aldrich (Sigma Aldrich, Saint. Louis, MO, USA) and applied for contact angle tests.

## 2.2. Preparation of photocatalysts

Polyaniline (PANI) was obtained by the oxidative polymerization method. Firstly, 90 cm<sup>3</sup> of 1 M hydrochloric acid and 0.1 cm<sup>3</sup> of aniline solution were mixed in a round-bottomed flask. The oxidant solution was then prepared by dissolving 0.25 g of ammonium persulfate in 30 cm<sup>3</sup> of 1M hydrochloric acid. The molar ratio of aniline to ammonium persulfate equaled 1:1. The polymerization reaction was carried out at 0°C for 24 hours. The resulting precipitate was centrifuged, washed three times with water and ethanol, and then dried for 24 hours at 70 °C.

To obtain PANI-TiO<sub>2</sub> composite, titanium(IV) oxide P25 was added into the acidic aniline solution before oxidation, and chemical oxidative polymerization was performed, as described above. The molar ratio of aniline to TiO<sub>2</sub> was equaled 1:5.

## 2.2. Preparation of photocatalytic gypsum plaster

The photocatalytic gypsum plaster was prepared by blending commercial gypsum plaster (Dolina Nidy), an addition of photocatalyst and distilled water in a quantity sufficient to obtain a paste form. The proportions of the individual ingredients were: 1.5 g of gypsum, 0.15 g of photocatalyst and 0.9 mL of distilled water. Two types of photocatalysts were used: the commercial TiO<sub>2</sub> (Evonik Aeroxide® TiO<sub>2</sub> P25) and PANI-TiO<sub>2</sub> in 10% wt. to the dry mass of the plaster. The blended gypsum was placed in a mold (30 mm diameter; 5 mm height) and dried at room temperature.

## 2.3. Characterization techniques

The chemical structure of samples was analyzed using FTIR Nicolet iS10 (Thermo Fisher Scientific Waltham, MA, USA) spectrometer at room temperature in the wavenumber range from 4000 to 400 cm<sup>-1</sup>. Each sample was scanned 64 times at a resolution of 4 cm<sup>-1</sup>.

XRD analysis was performed using the Rigaku Intelligent X-ray diffraction system SmartLab equipped with a sealed tube X-ray generator (a copper target; operated at 40 kV and 30 mA). Data was collected in the 2θ range of 5-80°. Scan speed and scan steps were 1° min<sup>-1</sup> and 0.01°, respectively. The analysis was based on the International Centre for Diffraction Data (ICDD) database. The crystallite size of the photocatalysts in the vertical direction to the corresponding lattice plane was determined using Scherrer's equation. Quantitative analysis, including phase composition with standard deviation, from the most intensive independent peak of each phase, was performed based on the ICDD database, using the Reference Intensity Ratio (RIR) method.

Nitrogen adsorption-desorption isotherms (BET method for the specific surface area) were measured using the Micromeritics Gemini V (model 2365) (Norcross, GA, USA) instrument at 77 K (liquid nitrogen temperature).

Diffuse reflectance spectra (DR) in the range of 300-800 nm were measured using ThermoScientific Evolution 220 Spectrophotometer (Waltham, MA, USA) equipped with PIN-757 integrating sphere.

The thermal stability of PANI-TiO<sub>2</sub> nanocomposite was studied with thermogravimetric analysis (TGA), using an SDT Q600 V20.9 Build 20 analyzer (New Castle, DE, USA). Sample of 7.5 mg mass was heated under a nitrogen atmosphere from 28 °C to 680 °C, with a heating rate of 50 °C·min<sup>-1</sup>.

The morphology of PANI-TiO<sub>2</sub> nanocomposite was studied using microscopy analysis on Tecnai F20 X-Twin (Fei Europe) microscope operated at 200 kV and Cs-corrected STEM (High Angle Annular DarkField, HAADF).

The photoluminescence (PL) spectra were recorded on a Perkin-Elmer LS 55 fluorescence spectrometer with a Xenon discharge lamp as the excitation source. The samples were excited at 250

nm in air at room temperature. A 290 nm cut off filter was used during measurements. The PL spectra were recorded in the range of 300 to 700 nm.

The contact angle test, by the sessile drop technique, was carried out to evaluate the hydrophilic/hydrophobic properties of the plaster surface. The analysis was performed using the Contact Angle System OCA 25 Instrument (DataPhysics, Germany). Pellet of gypsum plaster (diameter of 7 mm, the height of 4 mm) was prepared for contact angle test. On surface of the pellet, a 12  $\mu$ L droplet of liquid was placed, and the images were taken. Drops were dispensed automatically at medium speed using a 1 mL syringe. Ethylene glycol was used as a wetting liquid. The results of the contact angle were an average of six measurements.

#### 2.4. Photocatalytic activity

The photocatalytic activity was evaluated in a model reaction of phenol degradation under both UV-Vis and Vis light. As an irradiation source, 300 W Xenon lamp (LOT Oriel, Darmstadt, Germany) was used. For the visible light measurements, cut-off GG400 and GG420 filters (Optel, Opole, Poland) were used to obtain settled irradiation range above 400 nm and 420 nm, respectively. Photocatalyst at the content of 2 g·dm<sup>-3</sup> was added to 25 cm<sup>3</sup> of 20 mg·dm<sup>-3</sup> phenol solution. The obtained suspension was kept in darkness for 30 min under continuous stirring to provide adsorption-desorption stabilization. The irradiation intensity was controlled using optical power meter Hioki 3664 (Hioki E.R. Corporation, Nagano, Japan). The light flux in the range of 310-380 nm equaled to 30 mW·cm<sup>-2</sup>. The temperature of the reaction solution was kept at 20 °C using a water bath. Aliquots of 1.0 cm<sup>3</sup> of the reaction suspension were collected every 20 min and filtered through syringe filters ( $\varphi$  = 0.2  $\mu$ m) for the removal of photocatalysts particles. Phenol and intermediates were determined using a reversed-phase high-performance liquid chromatography (HPLC) system, equipped with a C18 chromatography column with bound residual silane groups (Phenomenex, model 00F-4435-E0) and a UV-Vis detector with a DAD photodiodes array model SPD-M20A, Shimadzu). The tests were carried out at 45 °C and under isocratic flow conditions of 0.3 cm<sup>3</sup>·min<sup>-1</sup> and volume composition of the mobile phase of 70% acetonitrile, 29.5% water and 0.5% orthophosphoric acid. Qualitative and quantitative analyses were performed based on previously made measurements of relevant substance standards and using the method of an external calibration curve.

The effect of charge carrier scavengers was examined by addition into the phenol solution (before introduction of the photocatalyst) 1 cm<sup>3</sup> of 500 mg·dm<sup>-3</sup> of *tert*-butyl alcohol (t-BuOH), silver nitrate (AgNO<sub>3</sub>), ammonium oxalate (AO) or benzoquinone (BQ), as hydroxyl radicals, superoxide, electron and hole scavengers, respectively.

Photocatalytic activity in the gaseous phase was analyzed, within the toluene decomposition, reaction. Test of toluene photocatalytic decomposition in a flat stainless steel reactor, with a working volume of 30 cm<sup>3</sup>, was performed. The reactor equipped with a quartz window, two valves, and a septum. The source of radiation was a set of 25 LEDs with emission range  $\lambda$  = 365-395 nm, maximum emission at  $\lambda_{\text{max}}$  = 380 nm,  $\lambda$  = 380-420 nm, maximum emission at  $\lambda_{\text{max}}$  = 400 nm,  $\lambda$  = 430-490 nm, maximum emission at  $\lambda_{\text{max}}$  = 460 nm. The intensity of the incident radiation measured by a Hioki 3664 meter with a Hioki 9741 sensor. For LEDs with emission range  $\lambda$  = 365-395 nm, the radiation flux at 380 nm was 2.5 mW·cm<sup>-2</sup>, for  $\lambda$  = 380-420 nm the radiation flux at 400 nm was 0.63 mW cm<sup>-2</sup>, for emission range  $\lambda$  = 430-490 nm the radiation intensity at 460 nm equalled 24.2 mW·cm<sup>-2</sup>. The toluene concentration was determined using a gas chromatograph (Clarus 500, PerkinElmer) equipped with flame ionization detector (FID) and DB-1 capillary column (30 m  $\times$  0.32 mm, film thickness 3.0  $\mu$ m). The samples (0.1 cm<sup>3</sup>) dosed by a gas-tight syringe (Hamilton). Hydrogen at the flow of 1.2 cm<sup>3</sup>·min<sup>-1</sup>, as the carrier gas, was used.

### 3. Results

#### 3.1. Characterization of photocatalysts

Figure 1 presented the FTIR spectra of PANI, PANI-TiO<sub>2</sub>, and TiO<sub>2</sub> samples. In the spectra, characteristic peaks attributed to both PANI and TiO<sub>2</sub>, were observed. The characteristic peak for

polyaniline at about  $3300\text{ cm}^{-1}$  corresponds to the stretching vibrations of the N-H groups. The band at  $1576\text{ cm}^{-1}$  corresponds to the stretching vibrations of C=N bonds in the quinone unit. Peaks at  $1496\text{ cm}^{-1}$  and  $825\text{ cm}^{-1}$  represent stretching vibrations of C=C bonds and C-H in benzene ring, respectively. Peaks at  $1307\text{ cm}^{-1}$  and  $1240\text{ cm}^{-1}$  results from C-N bond vibrations. The FTIR spectrum for unmodified titanium(IV) oxide includes an intense and wide peak in the range of  $400\text{--}900\text{ cm}^{-1}$ , which corresponds to Ti-O vibrations in the crystal structure. A wide band in the range of  $2900\text{--}3600\text{ cm}^{-1}$  correspond to O-H stretching vibrations of hydroxyl groups. Peak at  $1620\text{ cm}^{-1}$  represents bending vibrations of O-H hydroxyl groups resulting from the presence of water adsorbed on the semiconductor surface. Peaks at  $2361\text{ cm}^{-1}$  and  $2336\text{ cm}^{-1}$  correspond to vibrations of carbon(IV)oxide adsorbed on the surface of photocatalyst [2].

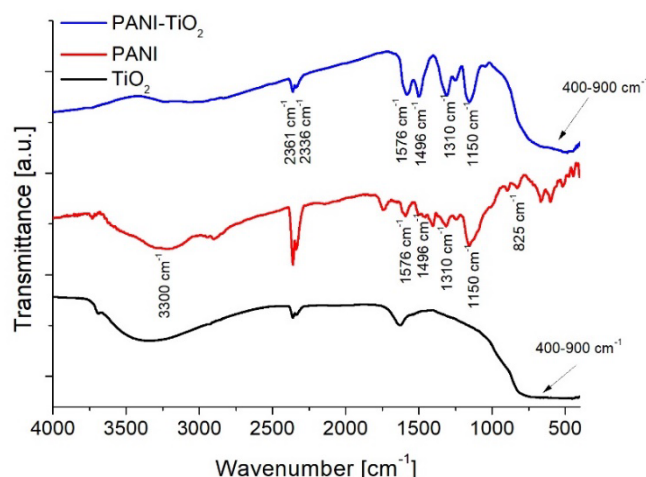


**Figure 1.** FT-IR spectra of  $\text{TiO}_2$ , PANI and PANI- $\text{TiO}_2$

**Table 1.** Crystalline structure and BET surface area of  $\text{TiO}_2$ , PANI and PANI- $\text{TiO}_2$

Sample label	BET surface area [ $\text{m}^2\cdot\text{g}^{-1}$ ]	Average crystallite size [nm]			
		Anatase		Rutile	
		Size [nm]	Phase content [%]	Size [nm]	Phase content [%]
PANI	11	-	-	-	-
$\text{TiO}_2$	55	$18.2 \pm 0.9$	$86.3 \pm 0.3$	$25.4 \pm 0.7$	$13.7 \pm 0.2$
PANI- $\text{TiO}_2$	55	$19.4 \pm 0.9$	$81.3 \pm 0.9$	$28.1 \pm 0.7$	$12.9 \pm 0.2$

XRD patterns of  $\text{TiO}_2$  and PANI- $\text{TiO}_2$  are shown, in Figure 2. As was expected for commercial  $\text{TiO}_2$  P25, two  $\text{TiO}_2$  crystal phases of anatase and rutile were distinguished. For both  $\text{TiO}_2$  bare and modified with PANI, the crystallite size for anatase and rutile equalled to 18 nm and ~25 nm, respectively. The phase content was also similar for PANI- $\text{TiO}_2$  and PANI. Anatase content equalled to  $86.3 \pm 0.3\%$  and  $81.3 \pm 0.9\%$  for  $\text{TiO}_2$  and PANI- $\text{TiO}_2$ , respectively, while rutile phase fluctuated from  $12.9 \pm 0.2\%$  to  $13.7 \pm 0.2\%$ . No peaks attributed to PANI, indicating low content and high dispersion or the amorphous form of polyaniline, were observed. The addition of polyaniline in the composite did not change the location and shape of  $\text{TiO}_2$  diffraction peaks. The BET surface did not change after the deposition of polymer particles and equalled for both photocatalysts to  $55\text{ m}^2\cdot\text{g}^{-1}$ . The BET surface area for pure PANI was  $11\text{ m}^2\cdot\text{g}^{-1}$ .



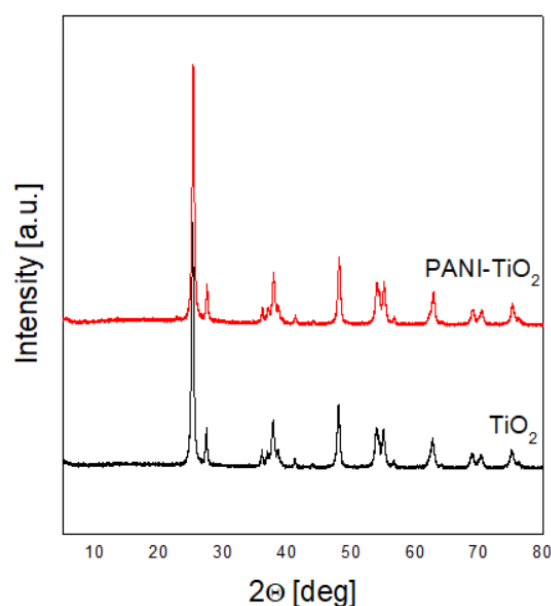


**Figure 2.** XRD patterns of  $\text{TiO}_2$  and  $\text{PANI-TiO}_2$

The UV-Vis absorption spectrum of pure  $\text{TiO}_2$ , PANI and  $\text{PANI-TiO}_2$  nanocomposite is presented in Figure 3 a. The bare  $\text{TiO}_2$  absorbed only UV light in the range of 200–400 nm, while PANI revealed absorption in visible light. The hybrid nanocomposite showed stronger absorption in the visible region compared to pure  $\text{TiO}_2$ . However, for  $\text{PANI-TiO}_2$  nanocomposite, we observe a decrease in absorption intensity in the range of 300–380 nm compared to bare  $\text{TiO}_2$ . A signal at around 440 nm for both PANI and  $\text{PANI-TiO}_2$  was observed. It indicated the polaron- $\pi^*$  transition of the quinoid ring [26]. The UV-Vis spectra suggested that PANI could be an effective photosensitizer for  $\text{TiO}_2$ .

The photoluminescence spectra of  $\text{TiO}_2$ , PANI and  $\text{PANI-TiO}_2$  nanocomposite were presented in Figure 3 b. All samples were at 250 nm wavelength excited. Three different maximum emission signals, in the PL spectra, at 405, 449 and 490 nm were identified for pure  $\text{TiO}_2$ . The peak at 3.06 eV (405 nm) corresponded to strong excitonic emission. The emission at 2.76 eV (449 nm) resulted from trap levels presence caused by  $\text{O}_2$  vacancies [27]. The peak at 2.53 eV (490 nm) related to the emission from  $\text{TiO}_2$  surface states [27]. Polyaniline PL spectrum is corresponding to the PL spectra presented in the literature [28,29]. Emission from the UV region, with the maximum at 395 nm, could be attributed to the  $\pi^*-\pi$  transition of the benzoic units in the conjugated polymer. In the visible region, two emission peaks at 487 nm and 605 nm were observed. The peak at 487 nm is related to de-excitation from the polaron band. Rohom et al. [28] also detected a similar emission peak at 613 nm however, its origin is not clarified. The PL spectrum of  $\text{PANI-TiO}_2$  hybrid nanocomposite is similar to the emission peak of polyaniline. This observation indicates that the presence of the conjugated polymer affects the light absorption properties of the nanocomposite.

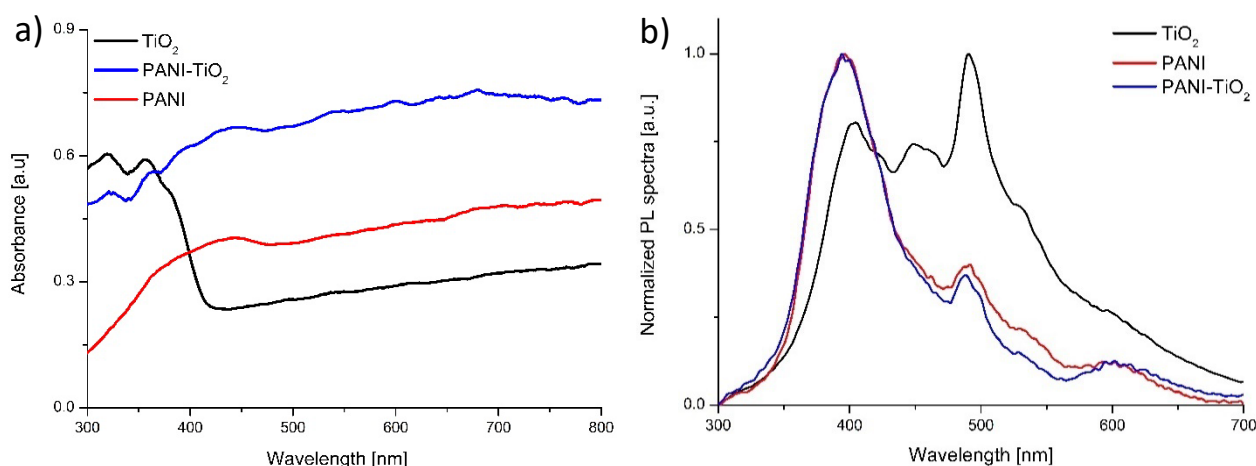


**Figure 3.** (a) DR/UV-Vis absorption spectra and (b) photoluminescence spectra of pure  $\text{TiO}_2$ , PANI and PANI- $\text{TiO}_2$  nanoparticles

An in-depth observation of the as-prepared samples by TEM analysis was conducted (see Fig. 4 a-c). Titanium(IV) oxide particles represented regular thin nanosheets of lamellar shape. Polyaniline was deposited on titanium(IV) oxide edged. Since titanium(IV) oxide P25 is highly crystalline and polyaniline represents no crystallographic structure, further FFT analysis for selected areas (magnification in Figure 4 c) that included both  $\text{TiO}_2$  and PANI was performed. Reflections of d spacing (see Figure 4 b) equaled to 0.35 nm and 0.24 nm corresponding to anatase  $\text{TiO}_2$  [110] and [202], respectively.

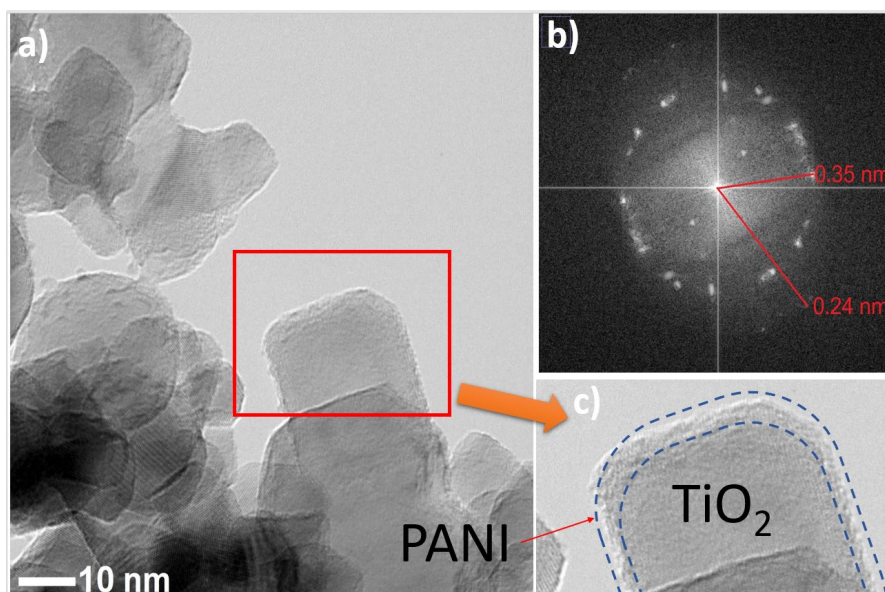


**Figure 4.** a) TEM image of PANI- $\text{TiO}_2$ , b) FFT analysis of PANI- $\text{TiO}_2$  nanocomposite, c) magnification on PANI- $\text{TiO}_2$  structure

The stability of PANI- $\text{TiO}_2$  nanocomposite using thermogravimetric analysis (TGA) was analyzed (see Figure 5). First weight loss (1), at the region up to 300 °C, is attributed to the volatilization of  $\text{H}_2\text{O}$  and HCl residuals. The second region (2) of sharp weight loss from 350 °C to 675 °C indicated polyaniline chains breakdown [30–32]. Above 675 °C, the weight of PANI- $\text{TiO}_2$  nanocomposite remained stable, indicating the complete decomposition of polyaniline. The final weight reduction of about 16% corresponded to theoretical polyaniline content in the hybrid nanocomposite.

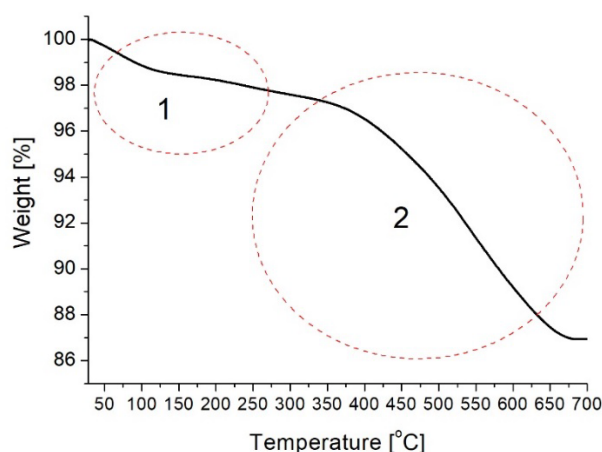


**Figure 5.** TGA curve of PANI-TiO<sub>2</sub> nanocomposite

### 3.2. Photocatalytic activity

To evaluate PANI-TiO<sub>2</sub> photocatalytic properties under UV-Vis and visible light degradation of phenol was studied. For visible-light experiments two cut-off filters GG400 ( $\lambda > 400$  nm) and GG420 ( $\lambda > 420$  nm) were used. The adsorption process proceeded for 30 min in a dark to obtain adsorption/desorption equilibrium conditions. The results of photocatalytic activity for PANI, TiO<sub>2</sub>, and PANI-TiO<sub>2</sub> nanocomposites in phenol degradation are presented in Table 2 and Figure 6. Bare TiO<sub>2</sub> revealed the highest photocatalytic activity under UV-Vis light among all examined photocatalysts. Bulk polyaniline exhibited low photocatalytic activity under UV-Vis light - only 6.5% of phenol degraded. The phenol degradation rate constant for PANI-TiO<sub>2</sub> nanocomposite equaled to  $(1.22 \pm 0.06) \cdot 10^{-2} \text{ min}^{-1}$  under UV-Vis irradiation. Deposition of PANI particles on TiO<sub>2</sub> surface reduced photocatalytic activity of TiO<sub>2</sub> under UV-Vis light. PANI particles may play the role of inner-filter blocking UV absorption of TiO<sub>2</sub>. Such an effect was observed in our previous results when the photocatalytic activity of TiO<sub>2</sub> modified with noble metals nanoparticles was lower than bare TiO<sub>2</sub> [33,34]. On the other hand, polyaniline enhanced photocatalytic activity of TiO<sub>2</sub> under wavelength longer than 420 nm. The phenol degradation rate constant for PANI-TiO<sub>2</sub> nanocomposite under visible light ( $\lambda > 420$  nm) -  $k$  equaled to  $(0.090 \pm 0.005) \cdot 10^{-2} \text{ min}^{-1}$ . Based on these results, PANI acts as a photosensitizer in the hybrid nanocomposite. Under visible light irradiation up to 400 nm ( $\lambda > 400$  nm), PANI-TiO<sub>2</sub> exhibited lower activity in phenol degradation compared to TiO<sub>2</sub> due to the possibility of activation of anatase-rutile heterojunction in the light range up to 400 nm. However, obtain results indicates that PANI improved TiO<sub>2</sub> activity in visible light, at a wavelength above 420 nm.

**Table 2.** Photocatalytic activity in reaction of phenol degradation

Sample label	Phenol degradation rate constant $k$ [ $10^{-2} \text{ min}^{-1}$ ]						
	UV-Vis	Vis $\lambda > 400 \text{ nm}$	Vis $\lambda > 420 \text{ nm}$	Scavenger (UV-Vis)			
				BQ	t-BuOH	AgNO <sub>3</sub>	AO
PANI	$0.090 \pm 0.010$	$0.010 \pm 0.001$	$0.040 \pm 0.002$	$0.050 \pm 0.002$	$0.050 \pm 0.002$	$0.400 \pm 0.020$	$0.190 \pm 0.010$
TiO <sub>2</sub>	$1.510 \pm 0.080$	$0.130 \pm 0.006$	$0.040 \pm 0.002$	$1.000 \pm 0.050$	$1.800 \pm 0.090$	$1.120 \pm 0.060$	$1.640 \pm 0.080$
PANI-TiO <sub>2</sub>	$1.220 \pm 0.060$	$0.020 \pm 0.001$	$0.090 \pm 0.005$	$1.230 \pm 0.060$	$1.060 \pm 0.050$	$1.210 \pm 0.060$	$0.740 \pm 0.040$



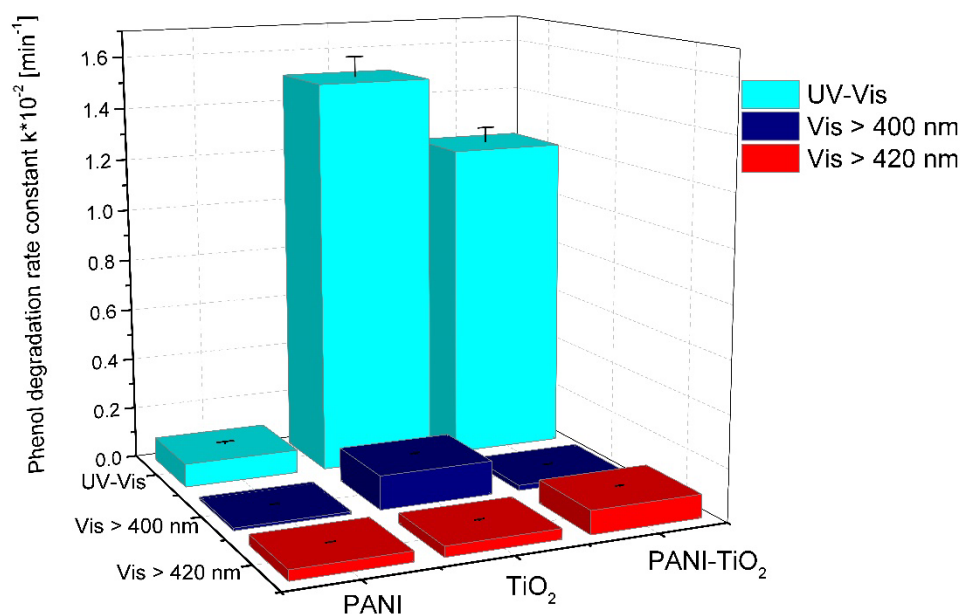
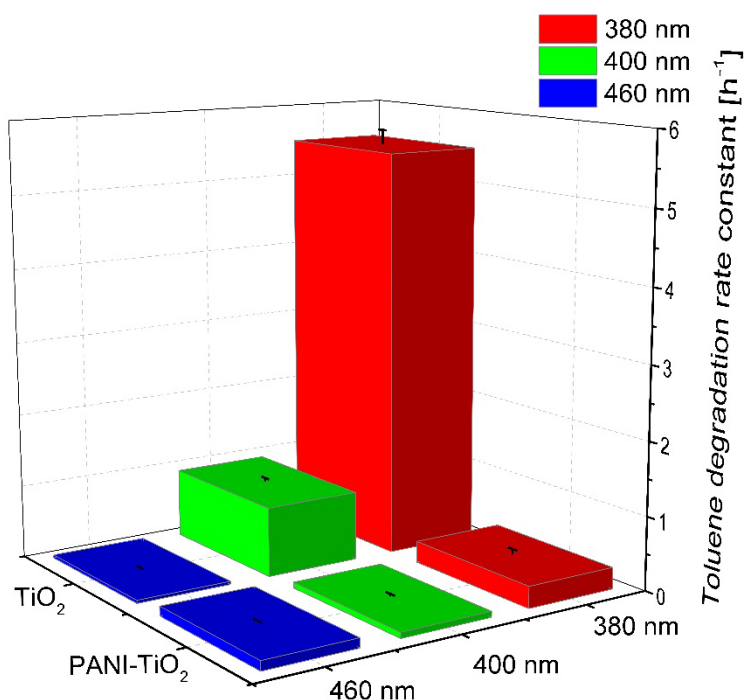


**Figure 6.** Phenol degradation of pure TiO<sub>2</sub>, PANI and PANI-TiO<sub>2</sub> nanocomposite under UV-Vis, Vis (>400 nm) and Vis (>420 nm)

To determine the mechanism of photocatalytic degradation of PANI-TiO<sub>2</sub> nanocomposite, the photocatalytic activity analysis, in the presence of scavengers, was performed. The results are presented in Table 2. Benzoquinone (BQ), *tert*-butanol (*t*-BuOH), silver nitrate (AgNO<sub>3</sub>), and ammonium oxalate (AO) were as O<sub>2</sub><sup>•−</sup> superoxide radical anions, OH<sup>•</sup> hydroxyl radicals, electrons and holes scavengers used, respectively. The degradation rate constants without scavengers under UV-Vis irradiation served as references. For PANI in the presence of BQ and *t*-BuOH a slight decrease in the phenol degradation rate constant to  $(0.050 \pm 0.002) \cdot 10^{-2} \text{ min}^{-1}$  was observed. However, in the presence of AgNO<sub>3</sub> or AO, the reaction rate constant increased to  $(0.40 \pm 0.02) \cdot 10^{-2} \text{ min}^{-1}$  and  $(0.19 \pm 0.01) \cdot 10^{-2} \text{ min}^{-1}$ , respectively. For pure PANI, the predominant role in mechanism of phenol photodegradation played direct redox reactions with electron-holes pairs over indirect oxidation with reactive oxygen species. Scavenging of both electron and holes inhibited e-h recombination. Phenol degradation mechanism for bare TiO<sub>2</sub> resulted from the generation of electrons and superoxide radical anions, as evidenced by decreased in the reaction rate constant from  $(1.51 \pm 0.08) \cdot 10^{-2} \text{ min}^{-1}$  to  $(1.00 \pm 0.05) \cdot 10^{-2} \text{ min}^{-1}$  and to  $(1.12 \pm 0.06) \cdot 10^{-2} \text{ min}^{-1}$  in the presence of BQ and silver nitrate, respectively. Scavenging of holes and hydroxyl radicals resulted in improvement of photocatalytic activity. For PANI-TiO<sub>2</sub> nanocomposite, the addition of BQ and AgNO<sub>3</sub> did not influenced on phenol degradation rate constant, while the presence of *t*-BuOH caused a slightly decrease in the constant rate. On the other hand, addition of AO as hole scavenger for PANI-TiO<sub>2</sub> resulted in decrease of phenol degradation. This suggests that for the nanocomposite, photogenerated holes played a crucial role in photodegradation mechanism.

Figure 7 is presented the results of photocatalytic activity for pure TiO<sub>2</sub> and PANI-TiO<sub>2</sub> nanocomposite in the gas phase. Pure TiO<sub>2</sub> showed the highest photocatalytic activity under UV-Vis light. Almost complete degradation of toluene in the gas phase proceeded in 30 min and 3h, using LEDs with  $\lambda_{\text{max}} = 380 \text{ nm}$  and  $\lambda_{\text{max}} = 400 \text{ nm}$  as an irradiation source, respectively. For PANI-TiO<sub>2</sub> nanocomposite under this condition, lower photocatalytic activity was obtained in comparison to pure TiO<sub>2</sub>. However, similar to the activity in the aqueous phase, when using irradiation of longer wavelengths ( $\lambda_{\text{max}} = 460 \text{ nm}$ ) an increase in photocatalytic activity for PANI-TiO<sub>2</sub> was observed. For hybrid photocatalyst irradiated using LEDs with  $\lambda_{\text{max}} = 460 \text{ nm}$ , the toluene degradation constant rate was  $0.130 \pm 0.010 \text{ h}^{-1}$ . In comparison, for bare TiO<sub>2</sub> the constant rate was  $0.043 \pm 0.005 \text{ h}^{-1}$  under the same conditions. Similarly, results were obtained in our previous study, on the degradation of toluene in the gas phase, over TiO<sub>2</sub> modified with Pt, Cu and Ag particles [33]. For LEDs with an

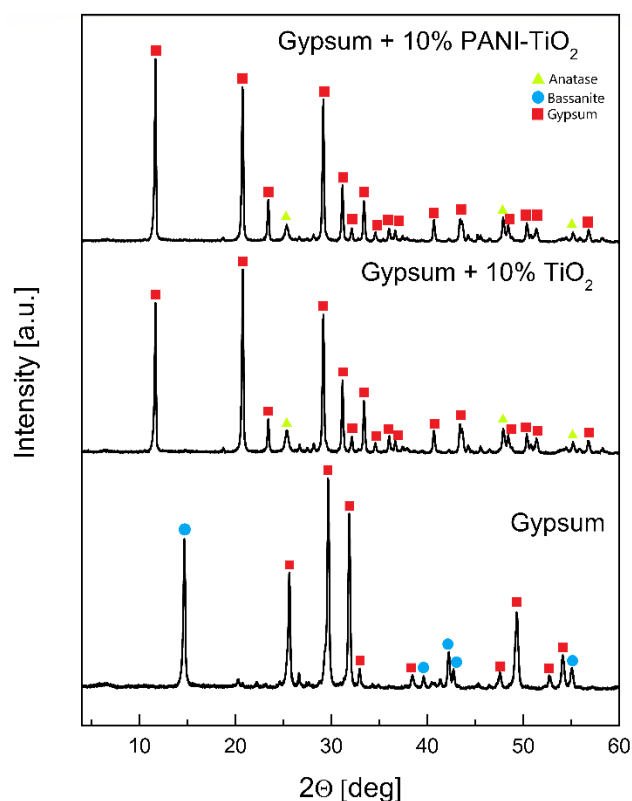
emission peak maximum at 400 nm (UV-Vis), bare titanium(IV) oxide exhibited significantly higher activity in comparison to metal-modified TiO<sub>2</sub>. However, under visible light irradiation with  $\lambda_{\text{max}} = 460$  nm, bare titanium(IV) oxide exhibited no activity, while metal-modified photocatalysts exhibited high activity resulted from plasmonic excitations of metal nanoparticles on TiO<sub>2</sub> surface [33].



**Figure 7.** Photocatalytic activity of pure TiO<sub>2</sub> and PANI-TiO<sub>2</sub> nanocomposite in the gas phase

#### 4. Photocatalytic gypsum plasters

The photocatalytic gypsum plasters were prepared by mixing gypsum, photocatalyst, and distilled water. The content of photocatalyst, TiO<sub>2</sub>, and PANI-TiO<sub>2</sub>, was 10% wt. for all samples. The thickness of the plasters was 5 mm. The X-ray diffraction patterns for pure gypsum and gypsum modified with TiO<sub>2</sub> and PANI-TiO<sub>2</sub> are presented in Figure 8. Only for the unmodified gypsum bassanite peaks at 14.71° [011] and 42.20° [51-2] were observed. The most intense peaks for pure gypsum at 25.60°, 29.66°, 31.85° and 49.31° corresponded to [13-1], [041], [221] and [260] gypsum structure planes, respectively. For gypsum samples modified with TiO<sub>2</sub> and PANI-TiO<sub>2</sub>, the 2 $\theta$  peaks at 25.36° and 47.87° confirmed the TiO<sub>2</sub> anatase [101] and [200] phase structures, respectively. The most intense peaks for gypsum loaded with TiO<sub>2</sub> and PANI-TiO<sub>2</sub> at 11.69°, 20.77°, 29.15° and 31.16° corresponded to gypsum [020], [12-1], [14-1] and [121] structure planes, respectively. Gypsum plaster with TiO<sub>2</sub> contained 8%  $\pm$  2% of anatase and 98%  $\pm$  8% of the gypsum phase. Gypsum plaster modified with PANI-TiO<sub>2</sub> had a lower anatase content than that modified with TiO<sub>2</sub>. The percentage content of phases in plasters loaded with PANI-TiO<sub>2</sub> was 2.80%  $\pm$  0.11% and 97.2%  $\pm$  0.8% for anatase and gypsum, respectively.

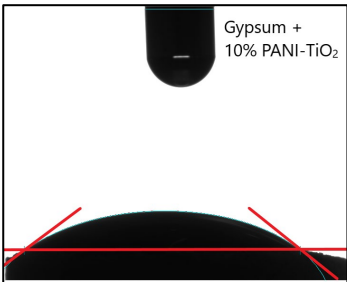


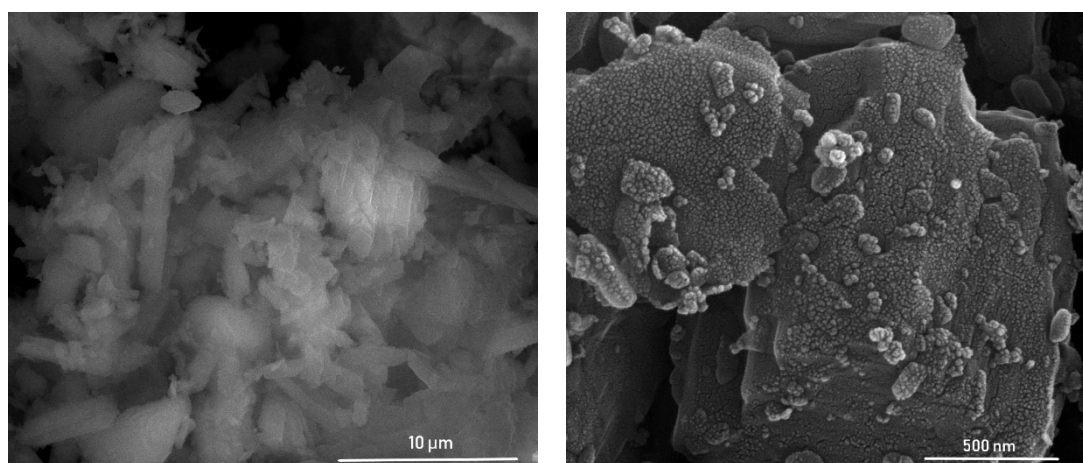
**Figure 8.** XRD patterns of gypsum and gypsum loaded with  $\text{TiO}_2$  or PANI- $\text{TiO}_2$

The analysis of the contact angle for gypsum samples was carried out to determine changes in surface properties of gypsum plaster after modification with a photocatalyst. Ethylene glycol was chosen as a liquid for the contact angle analysis. Based on the results presented in the Table 3, it was observed that the addition of photocatalysts changed the hydrophilic/hydrophobic properties of the plaster surfaces. Modified gypsum plasters possessed a smaller contact angle,  $20.6^\circ \pm 2.7^\circ$  and  $28.9^\circ \pm 0.6^\circ$  for gypsum loaded with 10% of  $\text{TiO}_2$  and 10% of PANI- $\text{TiO}_2$ , respectively than unmodified gypsum pellets –  $42.1^\circ \pm 1.9^\circ$ . The presence of conjugated polymer on the  $\text{TiO}_2$  surface may reduce the hydrophilic character of titanium(IV) oxide particles. As a result, the greater contact angle was for PANI- $\text{TiO}_2$  modified gypsum than for  $\text{TiO}_2$  modified gypsum due to the hydrophobic properties of the conjugated polymer.

Transmission electron microscopy analysis (see Figure 9) of gypsum loaded with PANI- $\text{TiO}_2$  photocatalyst showed coating of gypsum with a thin film of PANI- $\text{TiO}_2$  composite. The presence of PANI- $\text{TiO}_2$  on the gypsum surface is in agreement with the previous results in hydrophilic/hydrophobic properties of gypsum plaster after loading with PANI- $\text{TiO}_2$  nanocomposite.

**Table 3.** The contact angle results for gypsum and gypsum modified with TiO<sub>2</sub> or PANI-TiO<sub>2</sub>

Sample label	Contact angle [°]	
Gypsum	42.1 ± 1.9	
Gypsum + 10% wt. TiO <sub>2</sub>	20.6 ± 2.7	
Gypsum + 10% wt. PANI-TiO <sub>2</sub>	28.9 ± 0.6	

**Figure 9.** TEM images of gypsum loaded with PANI-TiO<sub>2</sub>

The model pollutant during the photocatalytic test was toluene, which was used at a concentration of 200 ppm in air. A summary of toluene degradation constant rate under UV and visible light irradiation for gypsum samples is presented in Figure 10. Gypsum plaster containing 10% of TiO<sub>2</sub> had the highest photocatalytic activity in the gas phase reaction, as it was previously described in paragraph 3.2 for pure TiO<sub>2</sub>. Toluene degradation rate constants were  $0.634 \pm 0.032 \text{ h}^{-1}$  for  $\lambda_{\text{max}} = 380 \text{ nm}$  and  $0.308 \pm 0.026 \text{ h}^{-1}$  for 460 nm maximum irradiation wavelength, respectively. For gypsum plaster modified with PANI-TiO<sub>2</sub> the constant rates were  $0.173 \pm 0.01 \text{ h}^{-1}$  and  $0.246 \pm 0.015 \text{ h}^{-1}$  for  $\lambda_{\text{max}} = 380 \text{ nm}$  and  $\lambda_{\text{max}} = 460 \text{ nm}$ , respectively. It is important to note that a decrease in degradation constant rate for gypsum modified with TiO<sub>2</sub> irradiated using LEDs with  $\lambda_{\text{max}} = 380 \text{ nm}$  and LEDs with light emission at  $\lambda_{\text{max}} = 460 \text{ nm}$  was observed. However, gypsum modified with 10% of PANI-TiO<sub>2</sub> photocatalytic activity under visible light irradiation ( $\lambda_{\text{max}} = 460 \text{ nm}$ ) was higher than for LEDs emitting UV light ( $\lambda_{\text{max}} = 380 \text{ nm}$ ). The obtained results are in good agreement with previously presented in this study for TiO<sub>2</sub> and PANI-TiO<sub>2</sub> results of photocatalytic activity in phenol and toluene degradation in aqueous and gaseous phases, respectively.

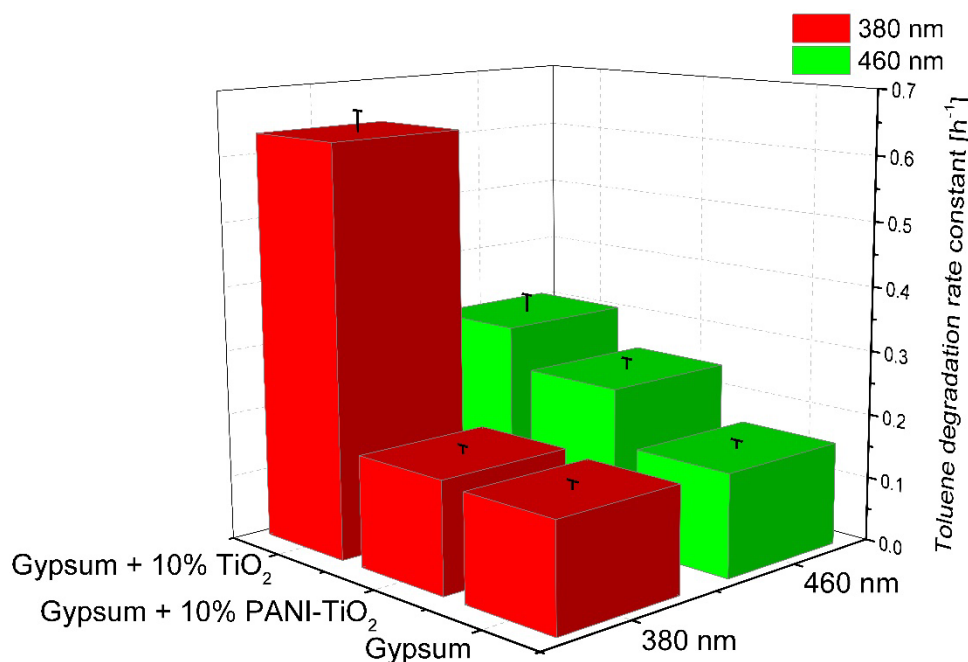


**Figure 10.** Toluene degradation in the presence of gypsum, gypsum loaded with TiO<sub>2</sub> and gypsum modified with PANI-TiO<sub>2</sub>

## 5. Discussion and concluding remarks

In summary, the PANI-TiO<sub>2</sub> nanocomposite was synthesized by an *in situ* chemical oxidative polymerization method. The photocatalytic activity of PANI-TiO<sub>2</sub> was evaluated in aqueous and gas phases. The obtained results indicate that polyaniline absorbs the visible light, and therefore, can be an effective photosensitizer of TiO<sub>2</sub> in a hybrid PANI-TiO<sub>2</sub> nanocomposite. As a result, the enhancement in photocatalytic activity for phenol and toluene degradation under visible light ( $\lambda > 420$  nm) was observed. On the other hand, under UV light, the photocatalytic activity for PANI-TiO<sub>2</sub> nanocomposite was significantly reduced, probably due to the blocking of active sites of titanium(IV) oxide by polyaniline. It was also observed that PANI photocatalytic activity mainly resulted from a direct electron-hole redox reactions over oxidation with reactive oxygen species.

Based on the obtained results, the mechanism of photocatalytic degradation over PANI-TiO<sub>2</sub> composites was proposed and presented in Figures 11-12. Under the visible light irradiation, with a wavelength longer than 420 nm, polyaniline acts as TiO<sub>2</sub> photosensitizer. The activation of PANI-TiO<sub>2</sub> nanocomposite proceeded through the excitation of electrons from HOMO to LUMO of polyaniline. Then, the excited electrons are transported into the TiO<sub>2</sub> conduction band (CB). Holes accumulated on the HOMO orbital of PANI, which can react with compounds adsorbed on the nanocomposite surface. Our results indicate that positive charge carriers are the main species responsible for degradation over PANI-TiO<sub>2</sub> nanocomposite.



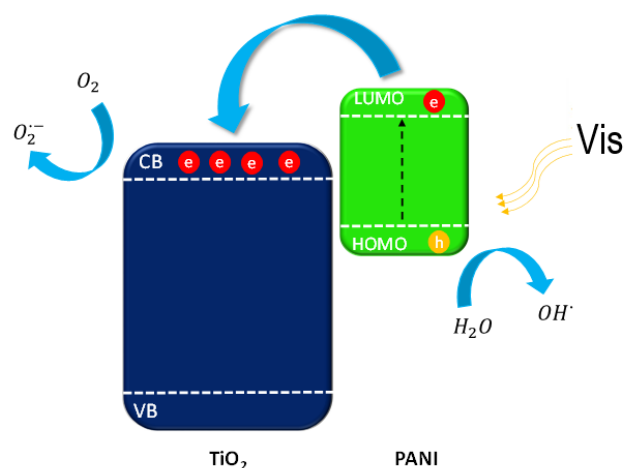


**Figure 11.** Mechanism of PANI-TiO<sub>2</sub> nanocomposite excitation under visible light

Under UV light, electrons from the TiO<sub>2</sub> valence band (VB) are excited to the conduction band (CB). Consequently, the traditional electron-hole pairs migration way would significantly accelerates the separation efficiency of charge carries by inner electric field established on the tightly contacted interface. The electrons located on the CB of TiO<sub>2</sub> were capture by oxygen (O<sub>2</sub>) dissolved in water to form O<sub>2</sub><sup>•−</sup> or further react with H<sup>+</sup> to yield •OH. The ROS of h<sup>+</sup>, •OH and O<sub>2</sub><sup>•−</sup> all participated in the photocatalytic degradation.

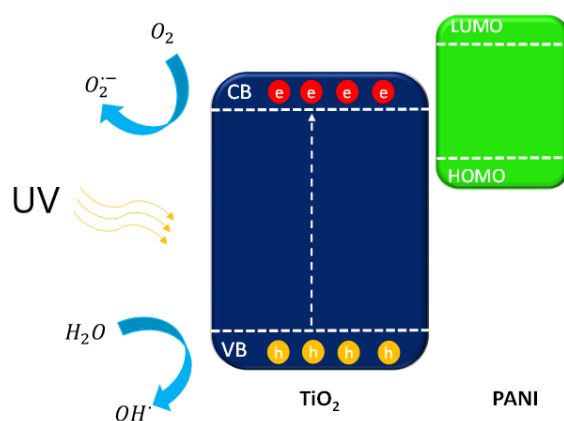


**Figure 12.** Mechanism of PANI-TiO<sub>2</sub> nanocomposite excitation under UV light

Nevertheless, the presence of polyaniline onto the TiO<sub>2</sub> surface might block titanium(IV) oxide active centers, which resulted in a decrease of photocatalytic activity under UV light. The deterioration of photocatalytic properties of PANI-TiO<sub>2</sub> nanocomposite under UV light may be a result of thick PANI layer or fine TiO<sub>2</sub> particle size, thus further studies should consider the effect of conjugated polymer content and the morphological properties of TiO<sub>2</sub> template on structure and photocatalytic activity of PANI-TiO<sub>2</sub> nanocomposites.

**Author Contributions:** conceptualization, AZ-J; methodology, AZ-J, IW; formal analysis, AS, IW, AZ-J; investigation, AS.; resources, AZ-J; writing—original draft preparation, AS, IW.; writing—review and editing, AZ-J, IW; supervision, AZ-J; project administration, AZ-J.; funding acquisition, AZ-J.

**Funding:** The research was financially supported by National Science Centre Poland, grant number NCN 2018/30/E/ST5/00845).

**Conflicts of Interest:** The authors declare no conflict of interest.

## References

- 1 Andreozzi, R.; Caprio, V.; Insola, A.; Marotta, R. Advanced Oxidation Processes (AOP) for Water Purification and Recovery. *Catal. Today* **1999**, *53* (1), 51–59. [https://doi.org/10.1016/S0920-5861\(99\)00102-9](https://doi.org/10.1016/S0920-5861(99)00102-9).
- 2 Guo, N.; Liang, Y.; Lan, S.; Liu, L.; Zhang, J.; Ji, G.; Gan, S. Microscale Hierarchical Three-Dimensional Flowerlike TiO<sub>2</sub> /PANI Composite: Synthesis, Characterization, and Its Remarkable Photocatalytic Activity on Organic Dyes under UV-Light and Sunlight Irradiation. *J. Phys. Chem. C* **2014**, *118* (32), 18343–18355. <https://doi.org/10.1021/jp5044927>.
- 3 Veres, Á.; Rica, T.; Janovák, L.; Dömök, M.; Buzás, N.; Zöllmer, V.; Seemann, T.; Richardt, A.; Dékány, I. Silver and Gold Modified Plasmonic TiO<sub>2</sub> Hybrid Films for Photocatalytic Decomposition of Ethanol under Visible Light. *Catal. Today* **2012**, *181*, 156–162. <https://doi.org/10.1016/j.cattod.2011.05.028>.
- 4 Fan, J. W.; Liu, X. H.; Zhang, J. The Synthesis of TiO<sub>2</sub> and TiO<sub>2</sub>-Pt and Their Application in the Removal of Cr (VI). *Environ. Technol.* **2011**, *32* (4), 427–437. <https://doi.org/10.1080/09593330.2010.501822>.
- 5 Espino-Estévez, M. R.; Fernández-Rodríguez, C.; González-Díaz, O. M.; Araña, J.; Espinós, J. P.; Ortega-Méndez, J. A.; Doña-Rodríguez, J. M. Effect of TiO<sub>2</sub>-Pd and TiO<sub>2</sub>-Ag on the Photocatalytic Oxidation of Diclofenac, Isoproturon and Phenol. *Chem. Eng. J.* **2016**, *298*, 82–95. <https://doi.org/10.1016/j.cej.2016.04.016>.
- 6 Gilson, R. C.; Black, K. C. L.; Lane, D. D.; Achilefu, S. Hybrid TiO<sub>2</sub> –Ruthenium Nano-Photosensitizer Synergistically Produces Reactive Oxygen Species in Both Hypoxic and Normoxic Conditions. *Angew. Chemie - Int. Ed.* **2017**, *56* (36), 10717–10720. <https://doi.org/10.1002/anie.201704458>.
- 7 Suwannaruang, T.; Kamonsuangkasem, K.; Kidkhunthod, P.; Chirawatkul, P.; Saiyasombat, C.; Chanlek, N.; Wantala, K. Influence of Nitrogen Content Levels on Structural Properties and Photocatalytic Activities of Nanorice-like N-Doped TiO<sub>2</sub> with Various Calcination Temperatures. *Mater. Res. Bull.* **2018**, *105* (February), 265–276. <https://doi.org/10.1016/j.materresbull.2018.05.010>.
- 8 Irie, H.; Watanabe, Y.; Hashimoto, K. Carbon-Doped Anatase TiO<sub>2</sub> Powders as a Visible-Light Sensitive Photocatalyst. *Chem. Lett.* **2003**, *32* (8), 772–773. <https://doi.org/10.1246/cl.2003.772>.
- 9 Rockafellow, E. M.; Stewart, L. K.; Jenks, W. S. Is Sulfur-Doped TiO<sub>2</sub> an Effective Visible Light Photocatalyst for Remediation? *Appl. Catal. B Environ.* **2009**, *91* (1–2), 554–562. <https://doi.org/10.1016/j.apcatb.2009.06.027>.
- 10 Chowdhury, P.; Moreira, J.; Gomaa, H.; Ray, A. K. Visible-Solar-Light-Driven Photocatalytic Degradation of Phenol with Dye-Sensitized TiO<sub>2</sub>: Parametric and Kinetic Study. *Ind. Eng. Chem. Res.* **2012**, *51* (12), 4523–4532. <https://doi.org/10.1021/ie2025213>.
- 11 Shang, J.; Zhao, F.; Zhu, T.; Li, J. Photocatalytic Degradation of Rhodamine B by Dye-Sensitized TiO<sub>2</sub> under Visible-Light Irradiation. *Sci. China Chem.* **2011**, *54* (1), 167–172. <https://doi.org/10.1007/s11426-010-4168-8>.
- 12 Yang, C.; Dong, W.; Cui, G.; Zhao, Y.; Shi, X.; Xia, X.; Tang, B.; Wang, W. Enhanced Photocatalytic Activity of PANI/TiO<sub>2</sub> Due to Their Photosensitization-Synergetic Effect. *Electrochim. Acta* **2017**, *247*, 486–495. <https://doi.org/10.1016/j.electacta.2017.07.037>.
- 13 Zhang, J.; Yao, Y.; Yang, H.; Xu, S.; Jiang, L.; Dan, Y. A New Carboxyl-Functionalized P3HT/TiO<sub>2</sub> Composite Photocatalyst: Preparation, Structure and Prompted Activity through Interfacial Engineering. *Proc. Nat. Res. Soc.* **2017**, *1*. <https://doi.org/10.11605/j.pnrs.201701003>.
- 14 Faisal, M.; Harraz, F. A.; Ismail, A. A.; El-Toni, A. M.; Al-Sayari, S. A.; Al-Hajry, A.; Al-Assiri, M. S. Polythiophene/Mesoporous SrTiO<sub>3</sub> Nanocomposites with Enhanced Photocatalytic Activity under Visible Light. *Sep. Purif. Technol.* **2018**, *190*, 33–44. <https://doi.org/10.1016/j.seppur.2017.08.037>.

- 15 Xu, J.; Hu, Y.; Zeng, C.; Zhang, Y.; Huang, H. Polypyrrole Decorated BiOI Nanosheets: Efficient Photocatalytic Activity for Treating Diverse Contaminants and the Critical Role of Bifunctional Polypyrrole. *J. Colloid Interface Sci.* **2017**, *505*, 719–727. <https://doi.org/10.1016/j.jcis.2017.06.054>.
- 16 Nguyen, H. Q.; Rainbolt, E. A.; Sista, P.; Stefan, M. C. Synthesis and Polymerization of Fused-Ring Thienodipyrrole Monomers. *Macromol. Chem. Phys.* **2012**, *213* (4), 425–430. <https://doi.org/10.1002/macp.201100608>.
- 17 Kang, E. T.; Neoh, K. G.; Tan, K. L. Polyaniline: A Polymer with Many Interesting Intrinsic Redox States. *Prog. Polym. Sci.* **1998**, *23* (2), 277–324. [https://doi.org/10.1016/S0079-6700\(97\)00030-0](https://doi.org/10.1016/S0079-6700(97)00030-0).
- 18 Ahmad, R.; Mondal, P. K. Adsorption and Photodegradation of Methylene Blue by Using PAni/TiO<sub>2</sub> Nanocomposite. *J. Dispers. Sci. Technol.* **2012**, *33* (3), 380–386. <https://doi.org/10.1080/01932691.2011.567172>.
- 19 Pan, H.; Liao, W.; Sun, N.; Murugananthan, M.; Zhang, Y. Highly Efficient and Visible Light Responsive Heterojunction Composites as Dual Photoelectrodes for Photocatalytic Fuel Cell. *Catalysts* **2018**, *8* (1). <https://doi.org/10.3390/catal8010030>.
- 20 Wei, J.; Zhang, Q.; Liu, Y.; Xiong, R.; Pan, C.; Shi, J. Synthesis and Photocatalytic Activity of Polyaniline-TiO<sub>2</sub> Composites with Bionic Nanopapilla Structure. *J. Nanoparticle Res.* **2011**, *13* (8), 3157–3165. <https://doi.org/10.1007/s11051-010-0212-z>.
- 21 Yu, Q. L.; Brouwers, H. J. H. Design of a Novel Photocatalytic Gypsum Plaster: With the Indoor Air Purification Property. *Adv. Mater. Res.* **2013**, *651* (2013), 751–756. <https://doi.org/10.4028/www.scientific.net/AMR.651.751>.
- 22 Zajac, K.; Janus, M.; Morawski, A. W. Improved Self-Cleaning Properties of Photocatalytic Gypsum Plaster Enriched with Glass Fiber. *Materials (Basel)*. **2019**, *12* (3). <https://doi.org/10.3390/ma12030357>.
- 23 Janus, M.; Zatorska, J.; Zająć, K.; Kusiak-Nejman, E.; Czyżewski, A.; Morawski, A. W. The Mechanical and Photocatalytic Properties of Modified Gypsum Materials. *Mater. Sci. Eng. B Solid-State Mater. Adv. Technol.* **2018**, 236–237 (November), 1–9. <https://doi.org/10.1016/j.mseb.2018.11.015>.
- 24 Gnayem, H.; Uvarov, V.; Lahad, O.; Sasson, Y. Hybrid Bismuth Oxyhalides@gypsum as Self-Cleaning Composites: Novel Aspects of a Sustainable Photocatalytic Technology for Solar Environmental Cleanup. *RSC Adv.* **2015**, *5* (82), 66650–66656. <https://doi.org/10.1039/c5ra09993e>.
- 25 Singh, V. P.; Mishra, D.; Kabachkov, E. N.; Shul, Y. M.; Vaish, R. The Characteristics of BiOCl/Plaster of Paris Composites and Their Photocatalytic Performance under Visible Light Illumination for Self-Cleaning. *Mater. Sci. Energy Technol.* **2020**, *3*, 299–307. <https://doi.org/10.1016/j.mset.2019.12.001>.
- 26 Xia, Y.; Wiesinger, J. M.; MacDiarmid, A. G.; Epstein, A. J. Camphorsulfonic Acid Fully Doped Polyaniline Emeraldine Salt: Conformations in Different Solvents Studied by an Ultraviolet/Visible/Near-Infrared Spectroscopic Method. *Chem. Mater.* **1995**, *7* (3), 443–445. <https://doi.org/10.1021/cm00051a002>.
- 27 Nair, R. V.; Gayathri, P. K.; Gummaluri, V. S.; Nambissan, P. M. G.; Vijayan, C. Large Bandgap Narrowing in Rutile TiO<sub>2</sub> Aimed towards Visible Light Applications and Its Correlation with Vacancy-Type Defects History and Transformation. *J. Phys. D. Appl. Phys.* **2018**, *51* (4). <https://doi.org/10.1088/1361-6463/aaa187>.
- 28 Rohom, A. B.; Londhe, P. U.; Mahapatra, S. K.; Kulkarni, S. K.; Chaure, N. B. Electropolymerization of Polyaniline Thin Films. *High Perform. Polym.* **2014**, *26* (6), 641–646. <https://doi.org/10.1177/0954008314538081>.
- 29 Banerjee, S.; Sarmah, S.; Kumar, A. Photoluminescence Studies in HCl-Doped Polyaniline Nanofibers. *J.*

- Opt.* **2009**, *38* (2), 124–130. <https://doi.org/10.1007/s12596-009-0011-z>.
- 30 Asha; Goyal, S. L.; Kumar, D.; Kumar, S.; Kishore, N. Synthesis and Characterization of Polyaniline/TiO<sub>2</sub> Composites. *Indian J. Pure Appl. Phys.* **2014**, *52* (5), 341–347.
- 31 Qi, Y. N.; Xu, F.; Sun, L. X.; Zeng, J. L.; Liu, Y. Y. Thermal Stability and Glass Transition Behavior of PANI/ $\alpha$ -Al<sub>2</sub>O<sub>3</sub> Composites. *J. Therm. Anal. Calorim.* **2008**, *94* (2), 553–557. <https://doi.org/10.1007/s10973-007-8626-2>.
- 32 Schnitzler, D. C.; Meruvia, M. S.; Hümmelgen, I. A.; Zarbin, A. J. G. Preparation and Characterization of Novel Hybrid Materials Formed from (Ti,Sn)O<sub>2</sub> Nanoparticles and Polyaniline. *Chem. Mater.* **2003**, *15* (24), 4658–4665. <https://doi.org/10.1021/cm034292p>.
- 33 Wysocka, I.; Markowska-Szczupak, A.; Szweda, P.; Ryl, J.; Endo-Kimura, M.; Kowalska, E.; Nowaczyk, G.; Zielińska-Jurek, A. Gas-phase Removal of Indoor Volatile Organic Compounds and Airborne Microorganisms over Mono- and Bimetal-modified (Pt, Cu, Ag) Titanium(IV) Oxide Nanocomposites. *Indoor Air* **2019**, No. March, 1–14. <https://doi.org/10.1111/ina.12595>.
- 34 Wysocka, I.; Kowalska, E.; Ryl, J.; Nowaczyk, G.; Zieli, A. Morphology, Photocatalytic and Antimicrobial Properties of TiO<sub>2</sub> Modified with Mono- and Bimetallic Copper, Platinum and Silver Nanoparticles. *Nanomaterials* **2019**.